Realization of a Fast Triple-Magic All-Optical Qutrit in ^{88}Sr

Maximilian Ammenwerth,[1,2] Hendrik Timme,[1,2] Flavien Gyger,[1,2] Renhao Tao,[1,2,3]
Immanuel Bloch,[1,2,3] and Johannes Zeiher[1,2,3,*]
[1]*Max-Planck-Institut für Quantenoptik, 85748 Garching, Germany*
[2]*Munich Center for Quantum Science and Technology (MCQST), 80799 Munich, Germany*
[3]*Fakultät für Physik, Ludwig-Maximilians-Universität, 80799 Munich, Germany*

(Received 4 November 2024; revised 17 June 2025; accepted 15 August 2025; published 2 October 2025)

The optical clock states of alkaline earth and alkaline earthlike atoms are the fundament of state-of-the-art optical atomic clocks. An important prerequisite for the operation of optical clocks is the magic trapping conditions where electronic and motional dynamics decouple. Here, we identify and experimentally demonstrate simultaneous magic trapping for two clock transitions in ^{88}Sr, realizing so-called triple-magic conditions at a specially chosen magic angle. Under these conditions, we operate an all-optical qutrit comprising the ground state $^1S_0$, and the two metastable clock states $^3P_0$ and $^3P_2$. We demonstrate fast optical control in an atom array using two- and three-photon couplings to realize high-fidelity manipulation between all qutrit states. At the magic angle, we probe the coherence achievable in magic-angle-tuned traps and find atom-atom coherence times between the metastable states as long as 715(30) ms. Our work opens several new directions, including qutrit-based quantum metrology on optical transitions and high-fidelity and high-coherence manipulation on the ^{88}Sr fine-structure qubit.

DOI: 10.1103/4kdl-xcwz

The vast majority of quantum information and quantum metrology protocols relies on binary representations of quantum information in terms of qubits. For example, efficient interferometry sequences have been devised in quantum metrology that translate phase information into measurable qubit populations [1–3]. Similarly, universal gate sets are known for qubits in quantum computation [4–8], and error correction architectures for qubits are well studied [9–12]. In practice, however, most quantum systems feature more states, which, if controlled, can serve as valuable resources [13–15]. Examples include motional states in trapped atoms or ions or additional internal states that extend the Hilbert space beyond the qubit subspace [16,17]. The optical clock states of ^{88}Sr are particularly interesting for applications in quantum computing [18,19] and metrology [3,20]. So far, most experiments have used the $^3P_0$ state, coupled to the electronic ground-state $^1S_0$ at a wavelength of 698 nm as an optical qubit. However, ^{88}Sr features a much richer structure, including the metastable $^3P_2$ state, which has a predicted natural lifetime exceeding 100 s, providing a second clock transition at 671 nm when coupled to the ground-state $^1S_0$ [21]. In principle, control over the three transitions coupling the metastable states $^3P_0$, $^3P_{2,m_j=0}$, and $^1S_0$ thus provides access to an all-optical qutrit, where all states are split by optical frequencies and can be coupled by laser drives. Compared to approaches with encodings in motional or hyperfine-structure states, the encoding of a qutrit of states split by optical transition frequencies offers new perspectives, including the tailored motional-state coupling [20], excellent state-preparation and measurement fidelities, and novel readout schemes of qubit states [22].

Experimentally, beyond the well-studied $^1S_0 \leftrightarrow {}^3P_0$ transition, coherent manipulation of the $^3P_2$ state was demonstrated [23]. Furthermore, recent work has explored the fine-structure qubit, which involves only the metastable clock states $^3P_0 \leftrightarrow {}^3P_{2,m_j=0}$ [24,25]. Here, the atoms were trapped at specific, experimentally fine-tuned magic trapping conditions, where differential light shifts induced by the trapping light vanish and internal and external motional degrees of freedom decouple. Such conditions have been demonstrated for various optical transitions in alkaline-earth (like) atoms by tuning the angle between the trap polarization and the quantization axis defined by a magnetic field [26–28], or ellipticity of the trap polarization with respect to the quantization axis [23,24,29].

Here, we significantly expand on previous work and implement a highly coherent all-optical qutrit in ^{88}Sr that is realized between both metastable clock states $^3P_0$, $^3P_{2,m_j=0}$ and the ground state $^1S_0$ with several novel features. *First*,

[*]Contact author: johannes.zeiher@mpq.mpg.de

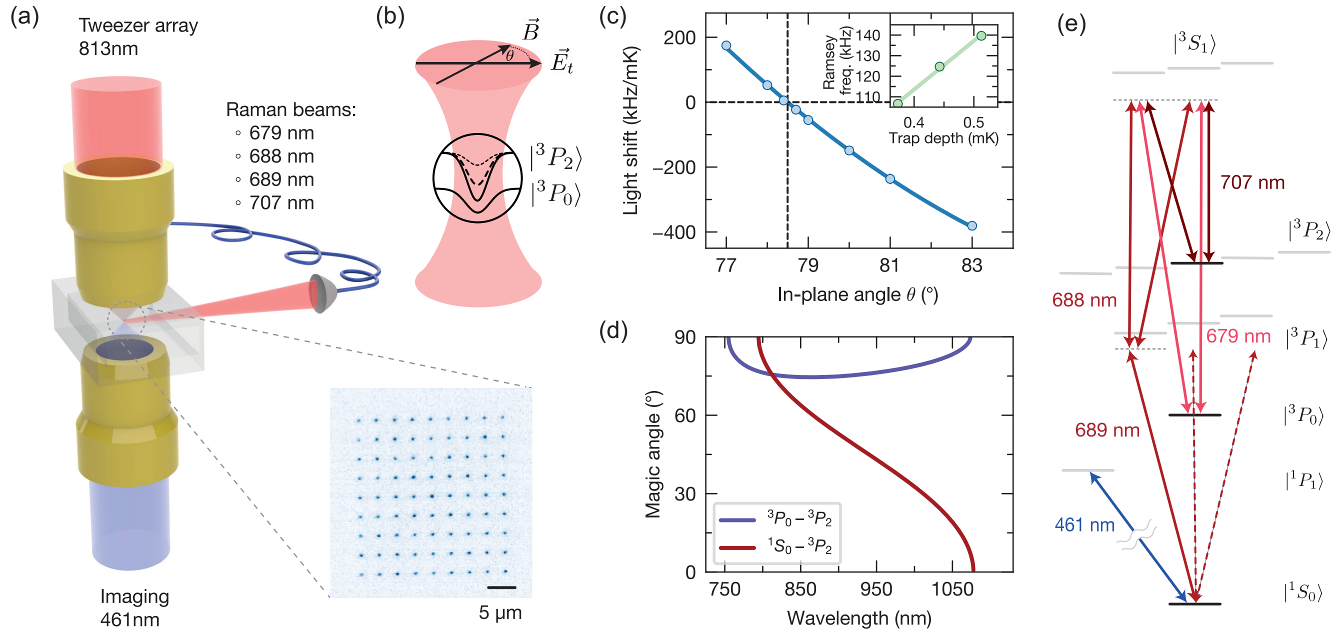

FIG. 1. Realization of triple-magic trapping conditions. (a) Main features of our experimental setup. We generate tweezer arrays at a wavelength of 813 nm using the top objective and image the atoms onto a camera using the bottom objective. Coherent control over the qutrit states is realized with four light fields at 679, 689, and 707 nm, which are delivered with common linear polarization from the same optical fiber and focussed onto the tweezer array. (b) Trapped in the optical tweezer, the two clock states *a priori* experience different trapping potential with a strong contribution of the tensor polarizability. By choosing a suitable angle of the magnetic field with respect to the tweezer polarization we equalize the polarizability as described in the main text. (c) The differential light shift between the clock states obtained from Ramsey spectroscopy is shown as a function of the magnetic field angle. The dependence of the differential light shift on tweezer depth is shown as a function of trap depth in the inset for a specific magnetic field in-plane angle of 81°. (d) The expected magic angle is shown as function of wavelength. At 813 nm the $^1S_0$ and $^3P_0$ state are scalar-magic, which therefore enables triple-magic conditions. (e) Level diagram of ^{88}Sr and the relevant wavelength used in this Letter. All light fields share a common linear polarization that is tilted with respect to the quantization axis, resulting in approximately equal projections for the π and $\sigma^{\pm}$ contributions. The polarizations and resulting couplings are discussed in the main text and Sec. A of SM [38]. To drive three-photon transitions, we choose a detuning in the vicinity of the $^1S_0 \leftrightarrow {}^3P_{1,m_j=-1}$ resonance.

we demonstrate the decoupling of all electronic qutrit states from motional states at magic trapping conditions in an optical tweezer array at 813 nm. *Second*, at magic conditions, we demonstrate coherent coupling of all involved qutrit states via multiphoton transitions [30], which allow for fast all-to-all Rabi coupling at small magnetic fields and optical powers compared to those typically required for coupling directly on optical clock transitions in ^{88}Sr [31]. In particular, our work significantly surpasses the coherence demonstrated recently for the $^1S_0 \leftrightarrow {}^3P_0$ transition using a Bose-Einstein condensate [32] and a thermal cloud of strontium atoms [33]. *Third*, we benchmark the coherence of the qutrit by characterizing the atom-laser coherence for all three couplings. We probe the fundamental limits of the qutrit coherence, which is susceptible to polarization gradients, via a detailed benchmarking of the coherence between the two metastable states $^3P_0$ and $^3P_{2,m_j=0}$ forming the fine-structure qubit in ^{88}Sr. We reach T_2 times up to $\tau_{dd} = 345(12)$ ms under continuous dynamical decoupling, significantly exceeding the previous state of the art on the fine-structure qubit. We furthermore find a lower bound of the atom-atom coherence time for the fine-structure qubit as long as $\tau_{at} = 715(30)$ ms, which is on par with coherence times achievable with ground hyperfine states in alkali atoms [34,35]. Our demonstration of long coherence times in polarizability-engineered tweezer traps substantiates the scalability of microscopically controllable neutral-atom quantum systems due to its applicability over a broad wavelength range. Furthermore, our work opens a new route to atomic state engineering using qutrits.

In our experiment, we operate a 9×9 site tweezer array in the focal plane of a high-resolution objective; see Fig. 1(a). To realize triple-magic trapping conditions, we choose our tweezer wavelength at 813 nm to provide magic trapping conditions between the ground state $^1S_0$ and the clock state $^3P_0$ [36,37]. In addition, we tune the polarizability of the $^3P_2$ state to the same value, which can be achieved in ^{88}Sr for the $^3P_{2,m_j=0}$ state by applying a magnetic field under an angle θ with respect to the linear tweezer polarization, in analogy to the known strategy for $^3P_1$ [26]. Because of the absence of total angular momentum J in the ground and $^3P_0$ clock states, their polarizability is unchanged by applying a magnetic field. We thus obtain the following expression for the tunable differential polarizability between $^1S_0$, $^3P_0$, and $^3P_{2,m_j=0}$:

$$\Delta\alpha = 3(\alpha_1 - \alpha_0)\sin^2\theta + \alpha_0, \quad (1)$$

with $\alpha_i = \alpha_{^3P_0} - \alpha_{^3P_{2,m_j=i}}$ being the polarizability difference between the $J = 0$ states and the $m_j = i$ Zeeman state of $^3P_2$. Using the known polarizability data for strontium, magic-angle tuning should enable the realization of magic trapping conditions across a wide range of wavelengths; see Fig. 1(d).

Our experimental sequence starts by loading the tweezer array from a two-stage magneto-optical trap, followed by a parity projection step to remove double occupancy in the tweezers. Subsequently, we image the occupation of the array by collecting the atomic fluorescence at a wavelength of 461 nm using a second objective and image it onto a qCMOS camera; see Fig. 1(a). During the imaging pulse, we additionally employ attractive Sisyphus cooling on the $^1S_0 \leftrightarrow {}^3P_1$ transition at 689 nm, resulting in high-fidelity, low-loss detection of the occupation of individual tweezers [46]. After this first image, we apply a sideband cooling pulse to cool the atoms in the radial direction, reaching a mean residual excitation number $\bar{n} = 0.14(4)$ [26] and correspondingly a motional ground-state occupation of 88(3)%. Subsequently, we apply a magnetic field with a strength of 19G in the horizontal plane at an angle θ between the linearly polarized tweezer array with electric field vector $\vec{E_t}$ and the magnetic quantization axis $\vec{B}$. At our typical trap depths of $U_0/k_B \leq 0.5$ mK, the chosen field strength is sufficient to define the quantization axis, which is required for magic-angle tuning. To couple $^1S_0$ to $^3P_0$ ($^3P_{2,m_j=0}$), we use a combination of three photons at 689, 688, and 679 nm (707 nm), coupling via the intermediate states $^3P_1$ with a detuning of $|\Delta_{689}| = 2\pi \times 6$ MHz (with respect to $^3P_{1,m_j=-1}$) and $^3S_1$ with a detuning of $|\Delta_{679}| = 2\pi \times 12$ GHz ($|\Delta_{707}| = 2\pi \times 12$ GHz); see Fig. 1(e). We couple the two metastable states $^3P_0 \leftrightarrow {}^3P_{2,m_j=0}$ off-resonantly via $^3S_1$ at Δ_{679} using two photons at 679 and 707 nm. To suppress differential phase noise, all lasers are locked to the same frequency comb and delivered to the experiment using the same polarization maintaining fiber. To locate the position of the magic angle, we first prepare the atoms in the $^3P_0$ clock state using a fast three-photon transfer [32,33], further described below. We then measure the light shift on the $^3P_0 \leftrightarrow {}^3P_{2,m_j=0}$ transition via Ramsey spectroscopy as a function of trap depth at various angles; see Fig. 1(c). We find that the differential polarizability vanishes at an angle of $\theta_m = 78.49(3)°$, in good agreement with the expected value considering a systematic uncertainty in the relative angle between tweezer polarization and magnetic field axis given by the coil orientation.

With the magic condition identified, we proceed to demonstrate fast, coherent, all-optical control of all transitions involved in the qutrit and benchmark the coherence times of all three couplings. In particular, we use combinations of three photons to couple from the ground state to both metastable states [32,33], and two photons to couple the two metastable states, as recently demonstrated in trapping conditions different from our experiment [24,25]. For the qutrit realized here, the combination of multiphoton processes allows for fast all-optical control at relatively modest external magnetic fields compatible with triple-magic angle tuning in experiments. The multicolor light field is impinging onto the array with linear polarization tilted approximately 55° out of the horizontal plane, which was chosen to equalize the polarization projection of the π and $\sigma^{\pm}$ components with respect to the horizontally set magnetic field and which maximizes the three-photon Rabi frequency in this configuration. On three-photon resonance, we observe corresponding Rabi oscillations with an initial contrast (at $\Omega_{^3P_0} t = \pi$) reaching up to 88% averaged over 118 repetitions of the experiment and the whole tweezer array; see Fig. 2(a). The extracted Rabi frequency of $\Omega_{^3P_0} = 2\pi \times 19.16(2)$ kHz for less than 10 mW total power in all three beams agrees well with analytic expectations and numerical simulations discussed in more detail in SM [38]. By modeling the Rabi oscillations in presence of experimental imperfections, we find that the observed dephasing is almost entirely accounted for by the independently measured laser phase noise [47]. Simulating a noise-free quantum system, we find that the limitations imposed by off-resonant scattering from excited states allow for substantially more Rabi cycles before the system dephases; see Fig. 2(a). In analogy to the coherent coupling to $^3P_0$, we also realize a coherent excitation of the $^3P_{2,m_j=0}$ state at the magic angle by substituting the photon at 679 nm with a photon at 707 nm; see Fig. 2(b). Performing high-resolution spectroscopy [shown in Fig. 2(d)], we find in this case a tweezer-dependent shift of the resonance position, which we attribute to small imperfections in the alignment of the array optics and a corresponding variation of the tweezer polarization angle across the array. These observations indicate the critical influence of precise alignment and the challenge to realize scalable tweezer arrays with excellent homogeneity. To characterize the coherence of the three-photon coupling, we measure the T_2^* time of the $^1S_0 \leftrightarrow {}^3P_0({}^3P_2)$ qubit in a Ramsey sequence, reaching $\tau_R^{^3P_0} = 3.4(2)$ ms $\left(\tau_R^{^3P_2} = 470(18)\ \mu\text{s}\right)$. Additionally, we employ a spin-echo sequence to mitigate the effect of polarization gradients and observe enhanced T_2 times of $\tau_{se}^{^3P_0} = 14.8(22)$ ms $\left(\tau_{se}^{^3P_2} = 8.1(24)\ \text{ms}\right)$. Our measurements, summarized in Fig. 2(e), demonstrate coherent all-to-all coupling between the qutrit states. We attribute the limited coherence time on

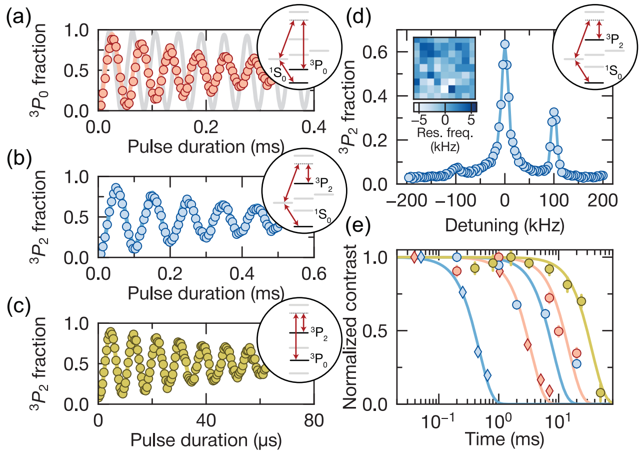

FIG. 2. Three-photon coupling between $^1S_0$ and $^3P_0$, $^3P_2$. (a) Rabi oscillations between $^1S_0$ and $^3P_0$. The red line shows simulation results of a simplified two-level model based on the measured in-loop laser phase noise without any free parameter. The gray line shows a noise-free simulation of the system taking all Zeeman substates and their couplings into account (see SM [38]). (b) We directly drive the $^1S_0 \leftrightarrow {}^3P_{2,m_j=0}$ transition with a three-photon pulse by exchanging the 679 nm light field with a corresponding beam at 707 nm. (c) Rabi oscillations on the fine-structure qubit under triple-magic conditions. We first initialize the qubit with a three-photon pulse into $^3P_0$ and then drive Rabi oscillations between the fine-structure states. (d) Tweezer-resolved three-photon spectroscopy on the $^1S_0 \leftrightarrow {}^3P_{2,m_j=0}$ transition, resulting in narrow resonance features with resolved red and blue motional sidebands. Extracting the center frequency for the transition for each tweezer (inset), we compute the tweezer-resolved polarization angle (see SM [38]). At a relative detuning of 100 kHz from the carrier we observe the radial sidebands of our tweezer array. (e) Coherence of the three-photon coupling. We obtain a T_2^* time of $\tau_R^{^3P_0} = 3.4(2)$ ms (red diamonds) for the $^1S_0 \leftrightarrow {}^3P_0$ three-photon coupling and T_2^* time of $\tau_R^{^3P_2} = 470(14)$ μs (blue diamonds) for the $^1S_0 \leftrightarrow {}^3P_2$ qubit, compatible with limitations caused by polarization gradients across the array as discussed in the main text. With a single spin echo we measure a T_2 time of $\tau_{se}^{^3P_0} = 14.8(22)$ ms (red circles) and $\tau_{se}^{^3P_2} = 8.1(24)$ ms (blue circles). For comparison, the T_2 time on the fine-structure states under equal conditions reaches $\tau_{se} = 36(2)$ ms (olive-green circles).

the $^1S_0 \leftrightarrow {}^3P_0$ coupling to laser phase noise, which is presented in SM [38].

With fast three-photon control on both ground-to-metastable transitions at hand, we now proceed to benchmark the fundamental coherence limit of the realized qutrit. Previous work [25] has raised concerns as to the achievable coherence times in angle-tuned tweezer potentials due to the presence of spatially dependent differential polarizabilities in tightly focused optical tweezers, which lead to temperature- and trap-depth-dependent spin motion coupling. To characterize the limitations imposed by magic-angle tuning and bypass the excess phase noise of the 688 nm laser (see SM [38]), we characterize the fine-structure (FS) qubit formed by both metastable states coupled on a coherent two-photon transition via the intermediate state $^3S_1$ in triple-magic conditions. For all measurements described in the following, we initialize the fine-structure qubit via a sideband-resolved three-photon π pulse on the $^1S_0 \leftrightarrow {}^3P_0$ transition, which preserves the motional ground state. Detection is similarly performed by controlled deexcitation of the clock state back into the ground state. Driving Rabi oscillations between $^3P_0$ and $^3P_{2,m_j=0}$, we extract a Rabi frequency of $\Omega_{\mathrm{FS}} = 2\pi \times 117$ kHz using only ~900 μW of power at 707 nm and ~850 μW of power at 679 nm; see Fig. 2(c). Here, the polarization setting that optimizes the coherent three-photon preparation is suboptimal, effectively lowering the achievable two-photon coupling on the FS qubit. However, we chose to use this setting for experimental convenience of not having to change the polarization between manipulation of the clock transitions and the FS transition. The FS qubit Rabi oscillations exhibit damping with a $1/e$ time of 50(1) μs, again compatible with estimates computed from the independently measured phase noise. To further substantiate that phase noise dominates the decay dynamics of the Rabi oscillations, we perform a spin lock measurement by first applying a $\pi/2$ pulse around the y axis, which aligns the state along the x axis in the state $|+\rangle = (|^3P_0\rangle + |^3P_{2,m_j=0}\rangle)/\sqrt{2}$ followed by a variable-time Rabi drive about the x axis [48]. In the absence of noise, the x drive is aligned and should stabilize the state $|+\rangle$. After a second $\pi/2$ pulse of variable phase, we perform a projective measurement of the populations in $^3P_0$ and $^3P_{2,m_j=0}$ and extract the contrast of the resulting Ramsey fringe. With this sequence, we observe a fast drop of the contrast with a time constant $\tau_{sl} = 49(4)$ μs in presence of the x drive, which indicates that currently excess phase noise at the Rabi drive is a major source of decoherence for our current laser system [49] and limits the observed contrast of our Rabi oscillations [50,51]. Here, the time constant τ_{sl} is obtained by fitting the resulting contrast with a function of the form $C(t) \propto \exp(-(t/\tau_{sl})^2)$. To further analyze the performance of the FS qubit, we also study its coherence in the absence of any driving light. First, we perform a standard Ramsey sequence with two $\pi/2$ pulses separated by a variable dark time and obtain a T_2^* time of $\tau_R = 463(7)$ μs. A tweezer-resolved analysis of the Ramsey oscillation frequency reveals that this rapid dephasing is dominated by inhomogeneities across the tweezer array; see Fig. 3(a). Such inhomogeneous shifts can be mitigated using dynamical decoupling techniques. Employing a standard XY-4 dynamical decoupling sequence [see Fig. 4(c)], we find a strongly boosted T_2 time of $\tau_{dd} = 345(12)$ ms, exceeding previous measurements in angle- or polarization-tuned magic optical traps by at least an order of magnitude [24,25]. We further study the

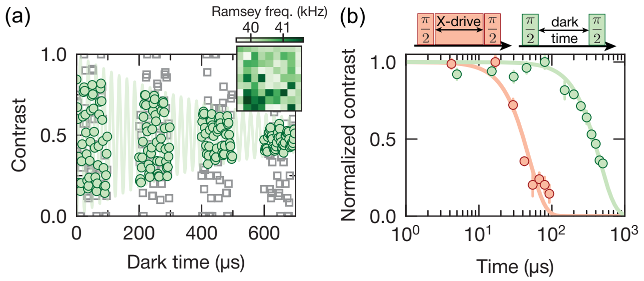

FIG. 3. Fine-structure qubit under triple-magic conditions. (a) Tweezer-resolved Ramsey measurement on the fine-structure qubit. The tweezer-averaged contrast (green circles) rapidly drops while individual tweezers (gray squares) show a high contrast. The tweezer-dependent Ramsey frequency (inset) is caused by a spatially varying polarization across the tweezer array (see SM [38]). Note that the single tweezer contrast decays on substantially longer timescales. (b) Comparison of the FS Ramsey measurement (green) with a spin-lock measurement (red). For both measurements, we apply two $\pi/2$ pulses along the y axis separated by a waiting time in the dark (green) or under a continuous Rabi drive along the x axis (red). The contrast of the spin-lock measurement decays significantly faster on a time scale of $\tau_{\mathrm{sl}} = 49(4)$ μs in agreement with the contrast decay in the Rabi oscillations, indicating limitations due to laser phase noise. For comparison, the T_2^* measurement on the fine-structure qubit shows a tweezer-averaged contrast decay with an extracted time of $\tau_R = 463(7)$ μs.

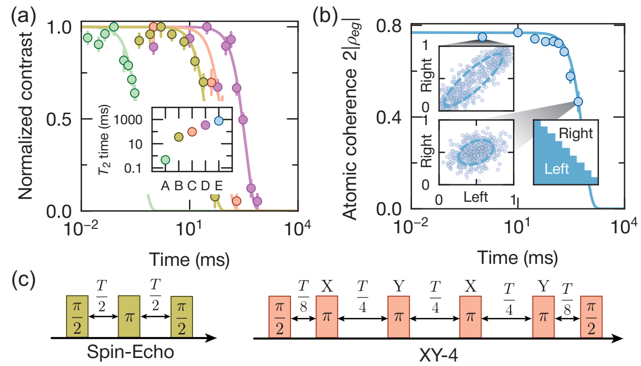

FIG. 4. Coherence of the fine-structure qubit. (a) Comparison of the fine-structure qubit T_2^* time and T_2 time measured with an XY-4 dynamical decoupling sequence. At a trap depth of 46 μK we obtain a T_2^* time of $\tau_R = 463(7)$ μs (light-green, inset A) and T_2 time of $\tau_{se} = 36(2)$ ms with a single spin echo (olive-green, inset B). Using an XY-4 dynamical decoupling sequence the T_2 time becomes $\tau_{dd'} = 97(6)$ ms (orange, inset C) and lowering the tweezer depth to about 5 μK, we boost the T_2 time to $\tau_{dd} = 346(37)$ ms (purple, inset D) setting a limit on the atom-laser coherence. The inset shows a summary of the measured coherence times including the atom-atom coherence time (blue, inset E). (b) To benchmark the atom-atom coherence we average a $g^{(2)}$ correlation function across subsets of our tweezer array to extract a lower bound for the atomic coherence (see SM [38]) and obtain a time constant of 715(30) ms. The correlations between the left and right half of the tweezer array are shown in the insets. (c) Pulse sequences used to measure the T_2 times using spin echo and XY-4 dynamical decoupling.

limits to the FS-qubit coherence by analyzing correlations between the qubit states measured within subsystems of the tweezer array; see Fig. 4. This measurement reveals the achievable atom-atom coherence, which can exceed the laser-atom coherence significantly [3]. We extract a decay time of $\tau_{at} = 715(30)$ ms from a fit to our data (see SM [38]), which can be interpreted as a lower bound to the atom-atom coherence achievable for the FS qubit in ^{88}Sr and on par with coherence times achieved, e.g., in hyperfine states of alkali atoms [35]. We expect that, with higher quality Rabi oscillations and more dynamical decoupling pulses, the coherence time can be boosted further.

Our demonstration of the all-to-all connectivity of the qutrit states under common conditions opens up new possibilities in quantum computing [52], quantum simulation, e.g., for the simulation of spin-1 systems [53–55], and metrology [56] with alkaline-earth atoms. Overcoming the technical limitations associated with laser noise opens the route to quantum computing and quantum simulation architectures involving fast transfers between the highly coherent strontium clock qubit [3] for storage and the fast FS qubit for operations. Realizing common trapping conditions for all qutrit states, comprising the clock states and the ground state, separated by optical frequencies, enables highly configurable interactions for quantum simulation experiments [57]. State-resolved readout of the qutrit population is feasible by imaging the ground-state population using fast, destructive fluorescence detection on the broad $^1S_0 \leftrightarrow {}^1P_1$ transition [58] combined with fast three-photon pulses to sequentially map the clock state populations to the ground state. Compared to the usually employed single-photon couplings, the three-photon coupling has the distinct advantage of operating at only low to moderate magnetic fields with high Rabi couplings at small required optical powers, dramatically improving the scaling perspectives of this approach (see SM for details [38]). Tuning the two-photon coupling from the clock states on resonance with the $^3P_1$ state, which subsequently decays to the ground state, can serve as a building block for recently proposed measurement-free quantum error correction [59], or highly controllable dissipative steps required for digital quantum simulation of open systems [60]. A reinitialization back to the clock states is subsequently possible via a fast three-photon pulse, exploiting the all-to-all connectivity of the qutrit. Going beyond the qutrit benchmarking, our promising results on the achievable coherence in angle-tuned magic traps open interesting perspectives for using the $^1S_0 \leftrightarrow {}^3P_{2,m_j=0}$ qubit, which can conveniently be tuned to magic conditions across a broad wavelength range, including IR wavelengths suitable for high-power ytterbium-doped fiber amplifiers. Sideband-resolved three-photon pulses on this transition and a dissipative state reset via the $^3P_1$ state enable direct sideband cooling, providing a novel route to ultralow-entropy states in assembled Hubbard systems. Finally, our demonstrated atom-atom coherence time involving the $^3P_2$ state opens promising perspectives for a variety of clock transitions in atoms trapped in nonscalar magic optical traps [56]. Thus, our work sets the stage for quantum metrology applications involving at least two clock transitions, which have been discussed in the context of uncovering slow temporal changes in fundamental constants [61]. To further suppress the effect of locally varying polarization, we envision trapping atom arrays in optical lattices instead of tweezer arrays [62–65]. Furthermore, single- and two-qubit gates on the FS qubit will benefit from erasure conversion based on the fluorescence detection of ground-state population [12,58,66]. Using combinations of single-qutrit rotations and Rydberg-mediated two-qubit gates, coupling either of the ^3P_J states to a Rydberg state, we envision creating and certifying three-dimensional entanglement [67].

Acknowledgments—We thank Ria Rosenauer and Kevin Mours for help with the 688 nm laser setup and Eran Reches and Lorenzo Festa for the code to estimate phase noise induced limitations. We acknowledge funding by the Max Planck Society (MPG) the Deutsche Forschungsgemeinschaft (DFG, German Research Foundation) under Germany's Excellence Strategy–EXC-2111–390814868, from the Munich Quantum Valley initiative as part of the High-Tech Agenda Plus of the Bavarian State Government, and from the BMBF through the programs MUNIQC-Atoms and MAQCS. This publication has also received funding under Horizon Europe programme HORIZON-CL4-2022-QUANTUM-02-SGA via the Project No. 101113690 (PASQuanS2.1). J. Z. acknowledges support from the BMBF through the program "Quantum technologies—from basic research to market" (SNAQC, Grant No. 13N16265). H. T., M. A., and R. T. acknowledge funding from the International Max Planck Research School (IMPRS) for Quantum Science and Technology. M. A. acknowledges support through a fellowship from the Hector Fellow Academy. F. G. acknowledges funding from the Swiss National Fonds (Fund No. P500PT_203162).

[1] N. Hinkley, J. A. Sherman, N. B. Phillips, M. Schioppo, N. D. Lemke, K. Beloy, M. Pizzocaro, C. W. Oates, and A. D. Ludlow, An atomic clock with 10^{-18} instability, Science **341**, 1215 (2013).

[2] E. Kessler, P. Kómár, M. Bishof, L. Jiang, A. Sørensen, J. Ye, and M. Lukin, Heisenberg-limited atom clocks based on entangled qubits, Phys. Rev. Lett. **112**, 190403 (2014).

[3] A. W. Young, W. J. Eckner, W. R. Milner, D. Kedar, M. A. Norcia, E. Oelker, N. Schine, J. Ye, and A. M. Kaufman, Half-minute-scale atomic coherence and high relative stability in a tweezer clock, Nature (London) **588**, 408 (2020).

[4] S. Bravyi and A. Kitaev, Universal quantum computation with ideal clifford gates and noisy ancillas, Phys. Rev. A **71**, 022316 (2005).

[5] M. Saffman, Quantum computing with atomic qubits and Rydberg interactions: Progress and challenges, J. Phys. B **49**, 202001 (2016).

[6] M. Saffman, T. G. Walker, and K. Mølmer, Quantum information with Rydberg atoms, Rev. Mod. Phys. **82**, 2313 (2010).

[7] S. J. Evered, D. Bluvstein, M. Kalinowski, S. Ebadi, T. Manovitz, H. Zhou, S. H. Li, A. A. Geim, T. T. Wang, N. Maskara, H. Levine, G. Semeghini, M. Greiner, V. Vuletić, and M. D. Lukin, High-fidelity parallel entangling gates on a neutral-atom quantum computer, Nature (London) **622**, 268 (2023).

[8] X.-F. Shi, Deutsch, toffoli, and cnot gates via Rydberg blockade of neutral atoms, Phys. Rev. Appl. **9**, 051001(R) (2018).

[9] A. G. Fowler, M. Mariantoni, J. M. Martinis, and A. N. Cleland, Surface codes: Towards practical large-scale quantum computation, Phys. Rev. A **86**, 032324 (2012).

[10] K. Sahay, J. Jin, J. Claes, J. D. Thompson, and S. Puri, High-threshold codes for neutral-atom qubits with biased erasure errors, Phys. Rev. X **13**, 041013 (2023).

[11] E. Knill and R. Laflamme, Theory of quantum error-correcting codes, Phys. Rev. A **55**, 900 (1997).

[12] Y. Wu, S. Kolkowitz, S. Puri, and J. D. Thompson, Erasure conversion for fault-tolerant quantum computing in alkaline earth Rydberg atom arrays, Nat. Commun. **13**, 4657 (2022).

[13] T. Roy, Z. Li, E. Kapit, and D. Schuster, Two-qutrit quantum algorithms on a programmable superconducting processor, Phys. Rev. Appl. **19**, 064024 (2023).

[14] A. R. Shlyakhov, V. V. Zemlyanov, M. V. Suslov, A. V. Lebedev, G. S. Paraoanu, G. B. Lesovik, and G. Blatter, Quantum metrology with a transmon qutrit, Phys. Rev. A **97**, 022115 (2018).

[15] S. Omanakuttan, V. Buchemmavari, J. A. Gross, I. H. Deutsch, and M. Marvian, Fault-tolerant quantum computation using large spin-cat codes, PRX Quantum **5**, 020355 (2024).

[16] L. H. Bohnmann, D. F. Locher, J. Zeiher, and M. Müller, Bosonic quantum error correction with neutral atoms in optical dipole traps, Phys. Rev. A **111**, 022432 (2025).

[17] M. Ringbauer, M. Meth, L. Postler, R. Stricker, R. Blatt, P. Schindler, and T. Monz, A universal qudit quantum processor with trapped ions, Nat. Phys. **18**, 1053 (2022).

[18] N. Schine, A. W. Young, W. J. Eckner, M. J. Martin, and A. M. Kaufman, Long-lived Bell states in an array of optical clock qubits, Nat. Phys. **18**, 1067 (2022).

[19] I. S. Madjarov, J. P. Covey, A. L. Shaw, J. Choi, A. Kale, A. Cooper, H. Pichler, V. Schkolnik, J. R. Williams, and M. Endres, High-fidelity entanglement and detection of alkaline-earth Rydberg atoms, Nat. Phys. **16**, 857 (2020).

[20] A. L. Shaw, R. Finkelstein, R. B.-S. Tsai, P. Scholl, T. H. Yoon, J. Choi, and M. Endres, Multi-ensemble metrology by programming local rotations with atom movements, Nat. Phys. **20**, 195 (2024).

[21] J. Trautmann, D. Yankelev, V. Klüsener, A. J. Park, I. Bloch, and S. Blatt, $^1S_0 - {}^3P_2$ magnetic quadrupole transition in neutral strontium, Phys. Rev. Res. **5**, 013219 (2023).

[22] Z. K. Minev, S. O. Mundhada, S. Shankar, P. Reinhold, R. Gutiérrez-Jáuregui, R. J. Schoelkopf, M. Mirrahimi, H. J. Carmichael, and M. H. Devoret, To catch and reverse a quantum jump mid-flight, Nature (London) **570**, 200 (2019).
[23] V. Klüsener, S. Pucher, D. Yankelev, J. Trautmann, F. Spriestersbach, D. Filin, S. G. Porsev, M. Safronova, I. Bloch, and S. Blatt, Long-lived coherence on a μHz scale optical magnetic quadrupole transition, Phys. Rev. Lett. **132**, 253201 (2024).
[24] S. Pucher, V. Klüsener, F. Spriestersbach, J. Geiger, A. Schindewolf, I. Bloch, and S. Blatt, Fine-structure qubit encoded in metastable strontium trapped in an optical lattice, Phys. Rev. Lett. **132**, 150605 (2024).
[25] G. Unnikrishnan, P. Ilzhöfer, A. Scholz, C. Hölzl, A. Götzelmann, R. Gupta, J. Zhao, J. Krauter, S. Weber, N. Makki, H. Büchler, T. Pfau, and F. Meinert, Coherent control of the fine-structure qubit in a single alkaline-earth atom, Phys. Rev. Lett. **132**, 150606 (2024).
[26] M. Norcia, A. Young, and A. Kaufman, Microscopic control and detection of ultracold strontium in optical-tweezer arrays, Phys. Rev. X **8**, 041054 (2018).
[27] T. Ido and H. Katori, Recoil-free spectroscopy of neutral Sr atoms in the lamb-dicke regime, Phys. Rev. Lett. **91**, 053001 (2003).
[28] R. Yamamoto, J. Kobayashi, T. Kuno, K. Kato, and Y. Takahashi, An ytterbium quantum gas microscope with narrow-line laser cooling, New J. Phys. **18**, 023016 (2016).
[29] A. Cooper, J. P. Covey, I. S. Madjarov, S. G. Porsev, M. S. Safronova, and M. Endres, Alkaline-earth atoms in optical tweezers, Phys. Rev. X **8**, 041055 (2018).
[30] T. Hong, C. Cramer, W. Nagourney, and E. N. Fortson, Optical clocks based on ultranarrow three-photon resonances in alkaline earth atoms, Phys. Rev. Lett. **94**, 050801 (2005).
[31] A. Taichenachev, V. Yudin, C. Oates, C. Hoyt, Z. Barber, and L. Hollberg, Magnetic field-induced spectroscopy of forbidden optical transitions with application to lattice-based optical atomic clocks, Phys. Rev. Lett. **96**, 083001 (2006).
[32] J. He, B. Pasquiou, R. G. Escudero, S. Zhou, M. Borkowski, and F. Schreck, Coherent three-photon excitation of the strontium clock transition, Phys. Rev. Res. **7**, L012050 (2025).
[33] S. P. Carman, J. Rudolph, B. E. Garber, M. J. V. de Graaff, H. Swan, Y. Jiang, M. Nantel, M. Abe, R. L. Barcklay, and J. M. Hogan, Collinear three-photon excitation of a strongly forbidden optical clock transition, Phys. Rev. X **15**, 031051 (2025).
[34] H. Levine, D. Bluvstein, A. Keesling, T. T. Wang, S. Ebadi, G. Semeghini, A. Omran, M. Greiner, V. Vuletić, and M. D. Lukin, Dispersive optical systems for scalable Raman driving of hyperfine qubits, Phys. Rev. A **105**, 032618 (2022).
[35] D. Bluvstein *et al.*, Logical quantum processor based on reconfigurable atom arrays, Nature (London) **626**, 58 (2024).
[36] M. Takamoto, F.-L. Hong, R. Higashi, and H. Katori, An optical lattice clock, Nature (London) **435**, 321 (2005).
[37] A. D. Ludlow, M. M. Boyd, T. Zelevinsky, S. M. Foreman, S. Blatt, M. Notcutt, T. Ido, and J. Ye, Systematic study of the ^{87}Sr clock transition in an optical lattice, Phys. Rev. Lett. **96**, 033003 (2006).
[38] See Supplemental Material at http://link.aps.org/supplemental/10.1103/4kdl-xcwz, which includes Refs. [39–45], for details regarding the modeling of the three-photon coupling, the effect of laser phase noise and spatial polarization gradients, and the estimation of the atom-atom coherence time.
[39] A. Heinz, A. J. Park, N. Šantić, J. Trautmann, S. G. Porsev, M. S. Safronova, I. Bloch, and S. Blatt, State-dependent optical lattices for the strontium optical qubit, Phys. Rev. Lett. **124**, 203201 (2020).
[40] F. Reiter and A. S. Sørensen, Effective operator formalism for open quantum systems, Phys. Rev. A **85**, 032111 (2012).
[41] B. E. King, Angular momentum coupling and Rabi frequencies for simple atomic transitions, arXiv:0804.4528.
[42] J. D. Thompson, T. G. Tiecke, A. S. Zibrov, V. Vuletić, and M. D. Lukin, Coherence and Raman sideband cooling of a single atom in an optical tweezer, Phys. Rev. Lett. **110**, 133001 (2013).
[43] B. Richards and E. Wolf, Electromagnetic diffraction in optical systems, II. structure of the image field in an aplanatic system, Proc. R. Soc. A **253**, 358 (1959).
[44] R. B.-S. Tsai, X. Sun, A. L. Shaw, R. Finkelstein, and M. Endres, Benchmarking and fidelity response theory of high-fidelity Rydberg entangling gates, PRX Quantum **6**, 010331 (2025).
[45] E. Rubiola, *Phase Noise and Frequency Stability in Oscillators* (Cambridge University Press, Cambridge, England, 2008), 10.1017/cbo9780511812798.
[46] J. P. Covey, I. S. Madjarov, A. Cooper, and M. Endres, 2000-times repeated imaging of strontium atoms in clock-magic tweezer arrays, Phys. Rev. Lett. **122**, 173201 (2019).
[47] H. Ball, W. D. Oliver, and M. J. Biercuk, The role of master clock stability in quantum information processing, npj Quantum Inf. **2**, 16033 (2016).
[48] J. H. Bodey, R. Stockill, E. V. Denning, D. A. Gangloff, G. Éthier Majcher, D. M. Jackson, E. Clarke, M. Hugues, C. L. Gall, and M. Atatüre, Optical spin locking of a solid-state qubit, npj Quantum Inf. **5**, 95 (2019).
[49] M. Bishof, X. Zhang, M. J. Martin, and J. Ye, Optical spectrum analyzer with quantum-limited noise floor, Phys. Rev. Lett. **111**, 093604 (2013).
[50] M. L. Day, P. J. Low, B. White, R. Islam, and C. Senko, Limits on atomic qubit control from laser noise, npj Quantum Inf. **8**, 72 (2022).
[51] H. Nakav, R. Finkelstein, L. Peleg, N. Akerman, and R. Ozeri, Effect of fast noise on the fidelity of trapped-ion quantum gates, Phys. Rev. A **107**, 042622 (2023).
[52] R. Majumdar, S. Basu, S. Ghosh, and S. Sur-Kolay, Quantum error-correcting code for ternary logic, Phys. Rev. A **97**, 052302 (2018).
[53] J. Mögerle, K. Brechtelsbauer, A. T. Gea-Caballero, J. Prior, G. Emperauger, G. Bornet, C. Chen, T. Lahaye, A. Browaeys, and H. P. Büchler, Spin-1 haldane phase in a chain of Rydberg atoms, PRX Quantum **6**, 020332 (2025).
[54] C. L. Edmunds, E. Rico, I. Arrazola, G. K. Brennen, M. Meth, R. Blatt, and M. Ringbauer, Symmetry-protected topological Haldane phase on a qudit quantum processor, PRX Quantum **6**, 020349 (2025).

[55] K. Kumaran, F. Alam, N. Eassa, K. Ferris, X. Xiao, L. Cincio, N. Bronn, and A. Banerjee, Transmon qutrit-based simulation of spin-1 aklt systems, arXiv:2412.19786.

[56] T. Ishiyama, K. Ono, T. Takano, A. Sunaga, and Y. Takahashi, Observation of an inner-shell orbital clock transition in neutral ytterbium atoms, Phys. Rev. Lett. **130**, 153402 (2023).

[57] R. M. W. van Bijnen and T. Pohl, Quantum magnetism and topological ordering via Rydberg dressing near Förster resonances, Phys. Rev. Lett. **114**, 243002 (2015).

[58] L. Su, A. Douglas, M. Szurek, A. H. Hébert, A. Krahn, R. Groth, G. A. Phelps, O. Marković, and M. Greiner, Fast single atom imaging for optical lattice arrays, Nat. Commun. **16**, 1017 (2025).

[59] S. Heußen, D. F. Locher, and M. Müller, Measurement-free fault-tolerant quantum error correction in near-term devices, PRX Quantum **5**, 010333 (2024).

[60] J. T. Barreiro, M. Müller, P. Schindler, D. Nigg, T. Monz, M. Chwalla, M. Hennrich, C. F. Roos, P. Zoller, and R. Blatt, An open-system quantum simulator with trapped ions, Nature (London) **470**, 486 (2011).

[61] M. S. Safronova, D. Budker, D. DeMille, D. F. J. Kimball, A. Derevianko, and C. W. Clark, Search for new physics with atoms and molecules, Rev. Mod. Phys. **90**, 025008 (2018).

[62] A. W. Young, W. J. Eckner, N. Schine, A. M. Childs, and A. M. Kaufman, Tweezer-programmable 2d quantum walks in a hubbard-regime lattice, Science **377**, 885 (2022).

[63] S. Buob, J. Höschele, V. Makhalov, A. Rubio-Abadal, and L. Tarruell, A strontium quantum-gas microscope, PRX Quantum **5**, 020316 (2024).

[64] R. Tao, M. Ammenwerth, F. Gyger, I. Bloch, and J. Zeiher, High-fidelity detection of large-scale atom arrays in an optical lattice, Phys. Rev. Lett. **133**, 013401 (2024).

[65] F. Gyger, M. Ammenwerth, R. Tao, H. Timme, S. Snigirev, I. Bloch, and J. Zeiher, Continuous operation of large-scale atom arrays in optical lattices, Phys. Rev. Res. **6**, 033104 (2024).

[66] S. Ma, G. Liu, P. Peng, B. Zhang, S. Jandura, J. Claes, A. P. Burgers, G. Pupillo, S. Puri, and J. D. Thompson, High-fidelity gates and mid-circuit erasure conversion in an atomic qubit, Nature (London) **622**, 279 (2023).

[67] N. Friis, G. Vitagliano, M. Malik, and M. Huber, Entanglement certification from theory to experiment, Nat. Rev. Phys. **1**, 72 (2018).